

## HiSST: 4th International Conference on High-Speed Vehicle Science & Technology



22-26 September 2025, Tours, France

# Influence of surface imperfections on laminar-turbulent transition of high-speed flows

Juan Alberto Franco<sup>1</sup>, Stefan Hein<sup>2</sup>, Alexander Wagner<sup>3</sup>

## Abstract

The presence of surface imperfections can have an important effect on the expected laminar-turbulent transition location for supersonic and hypersonic devices, leading to the appearance of highly localised areas of heat flux augmentation. The study presented in this paper investigates numerically the boundarylayer stability characteristics of a supersonic flow (Mach number = 4.5) in the presence of a rectangular backward-facing step (BFS) placed on a semi-infinite flat plate. The location of the step is defined by the synchronisation point (SP) of a reference two-dimensional 2<sup>nd</sup> mode with a frequency of 90 kHz (synchronisation frequency). The influence of the step height is investigated by considering five different step heights. The stability analysis combines the Parabolized Stability Equations (PSE) and the Adaptive Harmonic Linearized Navier-Stokes (AHLNS) methods. The high-fidelity AHLNS approach simulates the linear spatial evolution of convective instabilities in the presence of surface imperfections, and it has been already extensively used in transonic applications. The AHLNS stability tool is perfectly suited for studies regarding the influence of two-dimensional surface imperfections on the laminar-turbulent transition location. The low computational requirements of the AHLNS method (compared with similar techniques as DNS (Direct Numerical Simulation)) allow the study of a relatively broad band of modes, with frequencies higher and lower than the synchronisation frequency. Similar to previous studies about surface imperfections, the results of the present investigation show that the backward-facing step amplifies the lower-frequency modes and damps the higher-frequency modes (with respect to the synchronisation frequency). This paper describes the first application of the AHLNS methodology for supersonic configurations and sets the path for future applications in the study of the influence of surface imperfections in high-speed flows.

**Keywords:** surface imperfection, AHLNS, laminar, transition

## Nomenclature

Latin

BFS – Backward-facing step

c – Phase speed

f - Frequency of the flow instability

H – Step height

SP – Synchronisation point

TS – Tollmien-Schlichting

Greek

 $\delta_{99}$  – Boundary-layer thickness

 $\alpha$  – Streamwise wavenumber

 $\beta$  – Spanwise wavenumber

 $\omega$  – Circular frequency

 $\Theta$  – Phase function

Superscripts

\* – Dimensional quantity

† – Complex conjugate

Subscripts

w – Wall

u - Upstream of the step

d - Downstream of the step

 $\infty$  – Free stream

<sup>&</sup>lt;sup>1</sup>Department of High-Speed Configurations, Institute of Aerodynamics and Flow Technology, German Aerospace Center (DLR), Bunsenstrasse 10, 37073 Göttingen, Germany, juan.franco@dlr.de

<sup>&</sup>lt;sup>2</sup>Department of High-Speed Configurations, Institute of Aerodynamics and Flow Technology, German Aerospace Center (DLR), Bunsenstrasse 10, 37073 Göttingen, Germany

<sup>&</sup>lt;sup>3</sup>Department of High-Speed Configurations, Institute of Aerodynamics and Flow Technology, German Aerospace Center (DLR), Bunsenstrasse 10, 37073 Göttingen, Germany

#### 1. Introduction

The location of the laminar-turbulent transition is a critical aspect in high-speed configurations, such as reentry vehicles. In contrast to subsonic applications, where the boundary-layer transition has its main impact on the increase in aerodynamic drag, in supersonic and hypersonic configurations the most important aspect is the heat flux. An earlier transition location means an increase in structural protection systems and, therefore a critical raise in weight.

Surface imperfections, such as steps, gaps, roughness, etc. have a direct impact on the boundary-layer transition [1]. These two-dimensional (2D) surface imperfections represent the joint between different elements of an aerodynamic vehicle. Their presence is, in many cases, unavoidable. Therefore, from a design point of view, it is critical to establish tolerance criteria for safe operations. From a physical point of view, these irregularities introduce large streamwise gradients in the flow that affect the growth of the flow instabilities that trigger the boundary-layer transition. Therefore, it is very important to understand the flow mechanisms that lead the laminar-turbulent transition process, and how these mechanisms interact with the surface imperfections.

Fong et al. [2, 3] studied numerically by means of DNS (Direct Numerical Simulation) the influence of the location of the roughness (here, a 2D bump) on the growth of a particular  $2^{nd}$  mode (with a frequency of 100 kHz) in a hypersonic flow (Mach number = 5.92). They placed the surface imperfection at the synchronisation point (SP) of that particular frequency (i.e. synchronisation frequency). The SP is defined as the location where, for a given frequency, the phase speed of the first mode  $1^{st}$  synchronises with that of the  $2^{nd}$  mode. For their particular study [2, 3], the  $1^{st}$  and  $2^{nd}$  modes are called fast (F) and slow (S) modes, respectively, following the work of Fedorov [4]. Fong et al. [2, 3] found that instabilities at frequencies higher than the synchronisation frequency are damped. On the other hand, perturbations at frequencies lower than the synchronisation frequency are amplified by the roughness. By varying the height of the roughness, they found that higher roughness heights lead to stronger amplification or stronger damping of the flow instabilities (depending of the roughness position). Moreover, they investigated the presence of a second roughness in order to optimise the damping mechanism.

Inspired by the works of Fong et al. [2, 3], Gong et al. [5] studied numerically (using DNS) a backward-facing step (BFS) placed in a supersonic flow (Mach number = 4.5). Their investigations showed similar conclusions: instabilities at frequencies higher than the synchronisation frequency are damped by the BFS, and instabilities at frequencies lower than the synchronisation frequency are amplified. A result to bear in mind is that there is a certain step height that is the most effective to delay the transition.

Recently, Mi et al. [6] conducted experiments on a BFS at hypersonic conditions (Mach number = 6). They made use of Temperature-Sensitive Paints (TSP) to trace the heat flux distribution, and Nanotracer-based Planar Laser Scattering (NPLS) and schlieren techniques to visualise the flow structures across the step. In their study, Mi et al. considered not only rectangular steps, but steps with a ramp placed at the step corner. Their study shows that the presence of the BFS can effectively reduce the heat flux density downstream of the step location and, therefore, delay transition.

The existence of global instabilities was considered by Yu et al. [7]. They studied numerically a supersonic (Mach number = 2.16) BFS using DNS and GSA (Global Stability Analysis). The appearance of stationary modes was identified by varying the step height. Although no transition was observed in their studies, they were able to identify also oscillatory unstable modes. Interestingly, none of the unstable modes were two-dimensional, but three-dimensional.

The work of Zhao et al. [8] showed that not only surface imperfections can alter the spatial evolution of the flow instabilities. For that purpose, they placed a temperature strip in a hypersonic flat-plate flow (Mach number = 6). Their numerical investigation using DNS and LST (local stability theory) describes how the relative location of the strip with respect to the SP affects significantly the growth of the  $2^{nd}$  mode. A heating strip placed upstream of the SP amplified the mode, while the mode is damped if the strip is placed downstream (similar to the impact of a surface imperfection). The effect is reversed if the heating strip is replaced by a cooling strip.

Our investigation is based on the work of Gong et al. [5]. The flow configuration replicates the scenario

Table 1. Free-stream conditions

$Re_{\infty}$	$Ma_{\infty}$	$T_{\infty}$
$7.2 \times 10^6 \text{ m}^{-1}$	4.5	65.15 K

used in their studies. Our aim is to show that the use of AHLNS can be an alternative to computationally more demanding tools (such as DNS) for the study of such type of flows. Moreover, we will provide some insights about the flow physics that arise due to the interaction of the  $2^{nd}$  modes with the BFS, and confirm the conclusions of the study of Gong *et al.* [5].

The next section describes the setup of our study and the tools that will be used for the base flow computations and the subsequent stability analysis. Section 3 includes the outcome of our investigations, and highlights some of the physical aspects involved in the results presented. Finally, Sect. 4 summarizes the main conclusions of this study.

#### 2. Problem formulation and numerical setup

The computational domain represents a flat plate without any external pressure gradient. A backward-facing step (BFS) is located 472.5 mm from the leading edge. This point corresponds to the SP of the reference  $2^{nd}$  mode (with a frequency of 90 kHz). Flow conditions of the free-stream are specified in Table 1. These free-stream parameters are indicated with the subscript  $\infty$ .  $Re_{\infty}$ ,  $Ma_{\infty}$ , and  $T_{\infty}$  stand for unit Reynolds number, Mach number and temperature of the incoming flow, respectively. The inflow of the computational domain is placed 200 mm downstream from the leading edge. A compressible self-similar laminar profile is imposed at the inflow, following the same procedure as described by Zhou et al. [9]. At the wall, the no-slip velocity condition is imposed, as well as the isothermal temperature  $T_w = 289.04$  K. The outflow and upper side of the domain are placed at  $x^* = 2000$  mm and  $y^* = 2000$  mm, respectively. This configuration is schematically represented in Fig. 1. Dimensional quantities are indicated by an asterisk \*.

Five different BFS have been chosen for this work. Their relative height is indicated in Table 2, where  $H^*$  is the dimensional step height, and  $\delta_{99}$  represents the boundary layer thickness  $(99\%u_\infty^*)$  at the step location  $x_c^*$  for the flat flat without a BFS. The steady laminar base flow is computed using the DLR-Navier Stokes solver TAU [10]. Block-structured grids have been used to mesh the computational domain shown in Fig. 1. After a thorough grid convergence study, the number of points in streamwise and wall-normal directions for case BFS100 are shown in Table 3. The rest of cases are computed using a similar amount of points, simply changing the number of points in wall-normal direction in order to accommodate the different step heights while keeping the same point distribution. Local refinement in wall-normal direction has been applied close to the solid wall. Moreover, grid points are clustered around

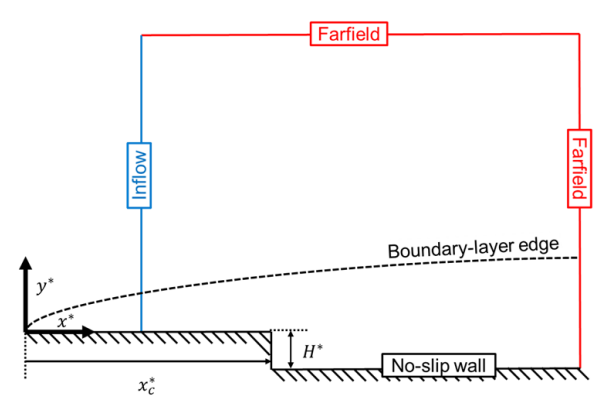


Fig 1. Computational domain and boundary conditions

Table 2. BFS cases and relative height

Cases	BFS20	BFS40	BFS60	BFS80	BFS100
$H^*/\delta_{99}$	0.2	0.4	0.6	0.8	1.0

the step location in streamwise direction. The minimum streamwise and wall-normal spacing at the step is  $3 \times 10^{-5}$  m and  $5 \times 10^{-5}$  m, respectively. The DLR-grid generator MEGACADS [11] has been used to generate the meshes.

#### 2.1. Linear stability analysis

The boundary-layer stability analysis has been done using two DLR codes: NOLOT-PSE [12] and AHLNS [13]. Both approaches are obtained from the Navier-Stokes (NS) equations linearized for small disturbance amplitudes. Flow quantities  $\mathbf{q}$  are decomposed into a steady laminar base flow  $\bar{\mathbf{q}}$  plus an unsteady disturbance flow component  $\tilde{\mathbf{q}}$ :

$$\mathbf{q}(\mathbf{x},t) = \bar{\mathbf{q}}(\mathbf{x}) + \varepsilon \tilde{\mathbf{q}}(\mathbf{x},t), \quad \varepsilon \ll 1.$$
 (1)

Here, t represents time. This flow decomposition is introduced into the NS equations, then the base state solution is subtracted and products of disturbance quantities are neglected. To further simplify the analysis, it is assumed that the base flow is homogeneous in spanwise direction z. Moreover, disturbances are assumed to be periodic in time t and in spanwise direction z. The wave-like representation of the flow instabilities is introduced here: the disturbance flow variables are decomposed into the product of an amplitude function  $\hat{\mathbf{q}}(x,y)$  and a wave function  $e^{i\Theta}$ , i.e.

$$\tilde{\mathbf{q}}(x, y, z, t) = \hat{\mathbf{q}}(x, y)e^{i\Theta}, \tag{2}$$

where the phase function is defined as

$$\Theta = \int \alpha(x')dx' + \beta z - \omega t. \tag{3}$$

Here  $\alpha$  stands for the complex-valued streamwise wavenumber, while real-valued parameters  $\beta$  and  $\omega$  represent the spanwise wavenumber and circular frequency of the disturbance, respectively. The streamwise wavenumber distribution  $\alpha(x)$  is computed iteratively for both PSE and AHLNS approaches, i.e.

$$\alpha_{new} = \alpha_{old} - i \frac{\int_0^\infty \left( \hat{\mathbf{q}}^{\dagger} \frac{\partial \hat{\mathbf{q}}}{\partial x} \right) dy}{\int_0^\infty \left( ||\hat{\mathbf{q}}||^2 \right) dy}, \tag{4}$$

with superscript  $\dagger$  referring to the complex conjugate. The adjustment of  $\alpha(x)$  is repeated iteratively until  $\alpha(x)$  can be considered as converged. Although the description of the PSE and AHLNS approaches is identical up to here, there are notable differences. Firstly, unlike to the PSE approach, the AHLNS method allows the streamwise wavenumber  $\alpha(x)$  and base flow quantities to rapidly vary in streamwise direction. Secondly, the AHLNS approach does not introduce any further simplification in the system of equations, i.e. all terms of the linearized Navier-Stokes (LNS) equations are kept. Therefore, the fully-elliptic system of equations of the AHLNS approach cannot be solved by a marching procedure (as it is done for PSE).

**Table 3.** Number of grid points for the steady laminar base flow computations. Subscripts u and d stand for upstream and downstream of the step location  $x_c^*$ 

Case	$nx_u \times ny_u$	$nx_d \times ny_d$
BFS100	$300 \times 325$	$1800 \times 425$

Typically, the presence of surface imperfections (e.g. steps) introduces locally large streamwise flow gradients. However, relatively far away from the irregularity (upstream and downstream) these streamwise variations remain small (compared with wall-normal gradients). Therefore, the most efficient procedure to compute the spatial evolution of convective instabilities (e.g. TS waves) consists on coupling the PSE and AHLNS methodologies in a multi-zonal approach: PSE is used in regions relatively far upstream and downstream of the surface imperfection, while AHLNS is used in the vicinity of such irregularity. The coupling of PSE and AHLNS approaches is straightforward, since both methodologies share the wave-like description of the flow instability (see eqn.(2)).

On the other hand, the number of grid points in streamwise x-direction required to compute an individual n-factor curve (see sec. 2.1.1) using the AHLNS approach is greatly reduced compared with similar methodologies as HLNS (Harmonic-LNS) or linear DNS (Direct Numerical Simulation). We remark that for HLNS and DNS methodologies no assumptions are made regarding the nature of the flow instabilities in x-direction. This aspect is discussed in detail in the work of Franco and Hein [13].

### 2.1.1. N-factor envelope

The n-factor measures the accumulated growth or decay of the disturbances. It is computed as

$$n(x) = \ln\left[A(x)/A_0\right],\tag{5}$$

where A(x) denotes the maximum amplitude, in wall-normal direction, of the streamwise velocity component of the corresponding instability mode at each location.  $A_0$  is the corresponding value of A(x) at the most upstream location where the disturbance starts to grow. Each n-factor curve is computed for a single mode defined by a particular frequency  $f^*$  and spanwise wavenumber  $\beta$ . The envelope of all n-factor curves considered is called the N-factor envelope, following the definition given by Arnal [14]:

$$N(x) = \max_{f,\beta} [n(x)] \tag{6}$$

## 3. Results

#### 3.1. Base flow

Figure 2 shows the nondimensional laminar steady base flow density contours and streamlines for the case BFS100. The contours of density indicate clearly the expansion fan that arises from the corner of the backward-facing step. The flow separates after the step, forming a recirculation zone that extends downstream up to the reattachment point. Readers can also notice the flow recompression downstream of the expansion fan.

### 3.2. Stability analysis

The stability analysis computes the spatial evolution of the individual two-dimensional  $2^{nd}$  modes, each one defined for a particular frequency  $f^*$  and spanwise wavenumber  $\beta$ . The reason of focusing on  $2^{nd}$  modes only is based on the results from Gong et al. [5]. They indicated that, for this configuration, the  $2^{nd}$  modes feature higher growth rates than the corresponding  $1^{st}$  modes. Moreover, the seminal work from Mack [15] points out that an individual two-dimensional ( $\beta = 0$ )  $2^{nd}$  mode exhibits larger growth rates than any of its counterpart three-dimensional ( $\beta \neq 0$ )  $2^{nd}$  modes. Our study encompasses a broadband spectrum of 41 frequencies, ranging from 70 kHz up to 110 kHz.

Figure 3 shows the phase speed c for the  $1^{st}$  and  $2^{nd}$  modes in the flat-plate configuration for three different frequencies: 90 kHz (synchronisation frequency), 100 kHz (higher-frequency), and 75 kHz (lower-frequency). The vertical dashed lines indicate the SP of each frequency (i.e. the location where the phase speed of the  $1^{st}$  and  $2^{nd}$  modes coincides). Our BFS is located at the SP of the synchronisation frequency. Therefore, for the higher-frequency mode, the BFS is placed downstream of its SP. The opposite holds for the lower-frequency mode: the BFS is placed upstream of its SP. The following analysis describes in more detail how the higher-frequency and lower-frequency modes are affected by the BFS.

Our domain of study for the stability analysis extends in streamwise direction from  $x^* = 0.2$  m up to  $x^* = 0.8$  m. The stability analysis couples the PSE and AHLNS methodologies. The PSE method is used upstream of the step location up to a certain location (here,  $x^* = 0.39$  m) where the streamwise

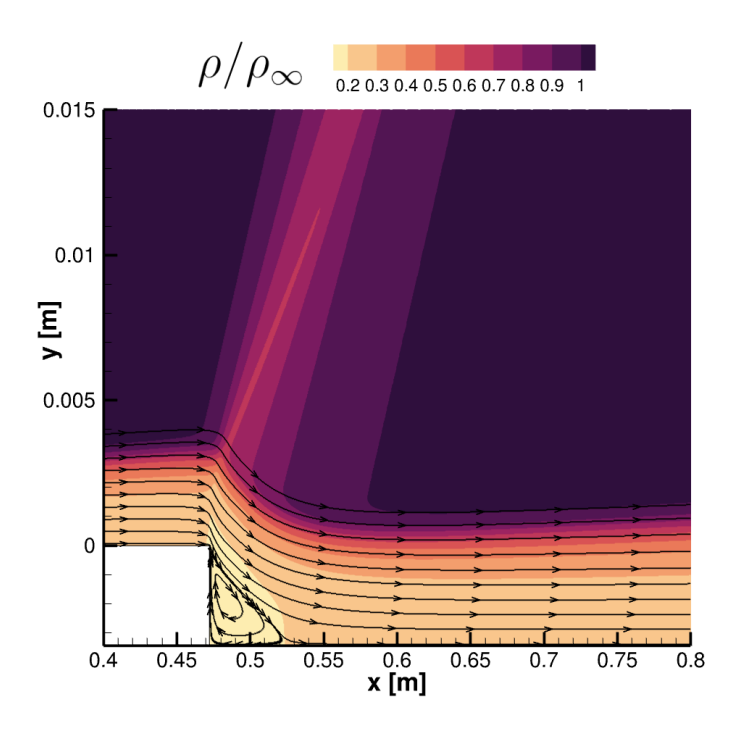


Fig 2. Base flow density contours and streamlines for the case BFS100. Axes are not to scale.

gradients remain small compared with wall-normal gradients. The AHLNS approach takes the PSE solution at  $x^* = 0.39$  m, and computes the spatial evolution of the flow instabilities up to the outflow (here,  $x^* = 0.8$  m). Although it is not included here, further PSE computations downstream of the outflow could be easily added for the amplified modes. For illustrative purposes, the DNS computations included in the work of Gong *et al.* [5] required about 1600 points in streamwise x-direction. Our AHLNS computations require 700 points only.

Figure 4-left shows the spatial evolution of an individual  $2^{nd}$  mode ( $f^* = 100 \text{ kHz}$ ) in the presence of the BFS100 step. The mode structure is dramatically affected by the backward-facing step. Upstream of the step, the mode increases its amplitude as long as it approaches the step. However, once the mode reaches the step, its amplitude is reduced significantly. The decrease in amplitude extends far downstream of the step. Moreover, the structure of the convective mode is affected also by the expansion fan that emerges from the step corner.

On the other hand, Fig. 4-right illustrates the development of another  $2^{nd}$  mode with a different frequency ( $f^* = 75 \text{ kHz}$ ) in the presence of the same BFS100 step. This mode shows similar features as already described for the previous higher-frequency mode ( $f^* = 100 \text{ kHz}$ , Fig. 4-left). In particular, the influence of the expansion fan that arises downstream of the step, and the reduction in amplitude in the region where the recirculation bubble is present. However, relatively far downstream of the step, both modes show a completely different behaviour. The lower-frequency mode ( $f^* = 75 \text{ kHz}$ ) experiences a significant amplification downstream of the step, while the higher-frequency mode, as mentioned before, is considerably damped.

The different behaviour of both modes is reflected in the individual n-factor curves depicted in Fig. 5. This figure compares the amplification of the two above-mentioned modes (with frequencies of 75 kHz and 100 kHz) for a flat plate (without any step) and in the presence of the BFS100 step. The amplitude of both modes remains almost unchanged upstream of the step (only a small reduction in n-factor close to the step for the 75 kHz mode). However, right downstream of the step, both modes experience a significant decrease in amplitude. In the case of the higher-frequency mode ( $f^* = 100 \text{ kHz}$ ), the decrease in amplitude extends far downstream of the step. Interestingly, the n-factor curve shows an oscillatory

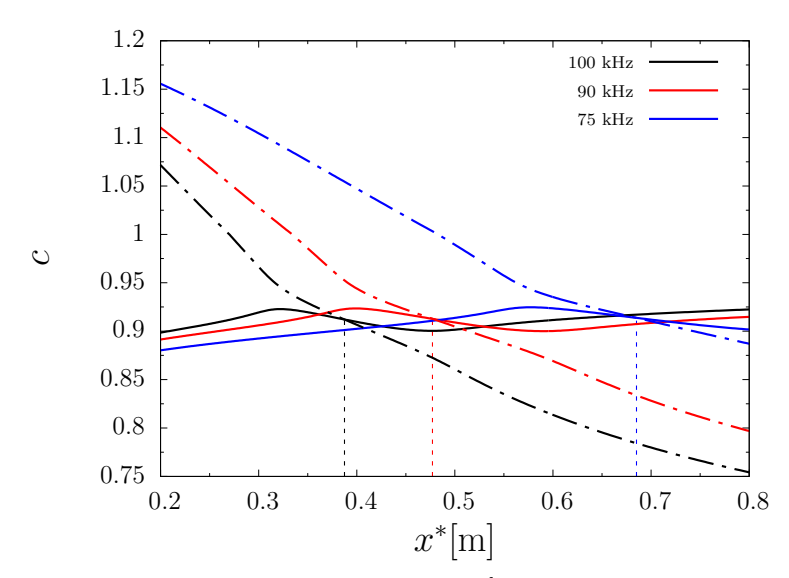


**Fig 3.** Phase speed c of  $1^{st}$  (point-dashed lines) and  $2^{nd}$  modes (solid lines) for frequencies 75 kHz, 90 kHz, and 100 kHz. Vertical dashed lines indicate the location of the synchronisation point for each frequency.

behaviour. This effect might indicate some type of interaction with the counterpart  $1^{st}$  mode. However, this point requires further analysis.

The lower-frequency mode ( $f^* = 75 \text{ kHz}$ ) experiences also a significant decrease in n-factor downstream of the step. However, contrary to the higher-frequency mode, it shows a large increase in growth rate downstream of the reattachment point of the recirculation bubble (see Fig. 2). The corresponding n-factor of this particular mode in the presence of the BFS100 step exceeds the values of n-factor of the same mode in the flat-plate configuration.

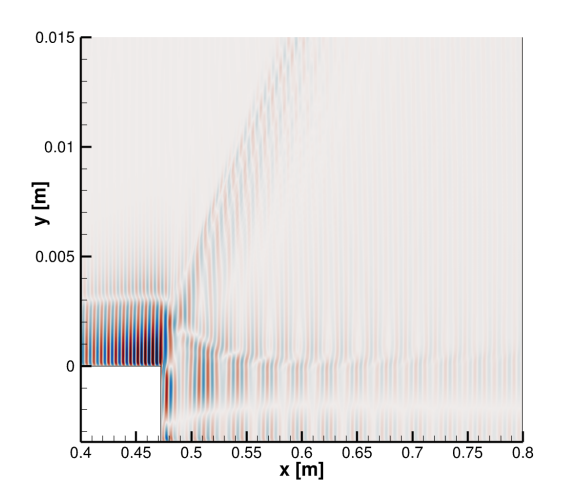
These results confirm the conclusions found in literature [2, 3, 5]: instabilities at frequencies higher than the synchronisation frequency are damped by the BFS, and instabilities at frequencies lower than the synchronisation frequency are amplified.

## 3.2.1. Influence of step height

The study of the higher-frequency and lower-frequency modes in the previous section is extended for the five step heights considered in this study, and it is depicted in Fig. 6. The effect of the BFS is similar for the five different steps: an almost negligible influence upstream of the step, followed by a significant reduction in amplitude in the immediate vicinity downstream of the step. The decrease in amplitude (and a particular oscillatory behaviour) for the higher-frequency mode (Fig. 6-right) is common for the five steps. For both the lower-frequency mode (Fig. 6-left), and the higher-frequency mode (Fig. 6-right), there is clearly a non-monotonic behaviour with step height. This result suggests (as discussed by Gong et al. [5]) that there is a certain step height that produces the maximum amplification / damping for the lower-frequency / higher-frequency modes, respectively.

### 3.2.2. N-factor envelope curves

The study for a particular lower-frequency and higher-frequency mode is extended for a relatively large spectrum of frequencies. This spectrum ranges from 70 kHz up to 110 kHz. Figure 7 shows the N-factor envelope curves for the five different BFS. Clearly, the characteristics of the N-factor curves far downstream of the step are dominated by the lower-frequency modes, showing a destabilising effect of the BFS compared with the flat-plate configuration. As expected, the step height produces a non-monotonic behaviour in the amplification curves, as described in the previous section. This result suggests that increasing the broadband spectrum of frequencies and the downstream extend of the computational domain, will contribute to a better understanding of the whole transition scenario and a better understanding of



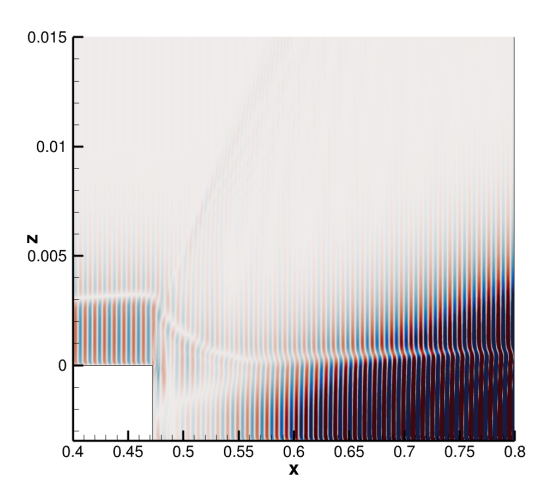


**Fig 4.**  $2^{nd}$  mode evolution ( $f^* = 100$  kHz-left,  $f^* = 75$  kHz-right) in the presence of the BFS100 step. Contours of the streamwise velocity component  $\tilde{u}$ . Axes are not to scale.

the influence of the BFS on the development of the  $2^{nd}$  modes.

#### 4. Conclusions

The influence of a backward-facing step (BFS) of different heights on the spatial development of  $2^{nd}$  modes on a supersonic flow (Mach number = 4.5) has been studied numerically. The stability analysis is done by coupling the PSE and AHLNS methods. A relatively large spectrum of 41 different frequencies has been considered. The results agree with previous investigations that made use of more computationally-demanding tools as DNS. The BFS has been placed at the synchronisation point (where  $1^{st}$  and  $2^{nd}$  mode has the same phase speed) for a particular frequency (synchronisation frequency). It has been shown that higher-frequency modes (with respect to the synchronisation frequency) are damped by the BFS, while lower-frequency modes are amplified. The study of the effect of step height has revealed a non-monotonic influence on the amplification/damping on the  $2^{nd}$  modes. However, for completeness of the study, a wider range of frequency spectrum and larger extension of the computational domain would be desirable. The lower computational requirements of the AHLNS approach, and easy coupling with PSE, makes this task relatively straightforward.

The AHLNS methodology has been extensively used for transonic applications in realistic airfoil geometries [16]. The flexibility of the code for the study of different types of surface imperfections (rectangular and rounded steps, gaps, humps, ramps, etc.) makes its application possible for parametric studies, where specific tolerance criteria for surface imperfections are required. This paper represents the first application of the AHLNS approach for supersonic flows and demonstrates its potential for application for high-speed flows.

Finally, we remark the need of these studies in order to enhance our knowledge in the understanding of how surface imperfections might alter the location of the boundary-layer transition, a key aspect for the design of current and future supersonic and hypersonic vehicles.

#### References

- [1] W. Ivison, C. Hambidge, M. McGilvray, J. Merrifield, and J. Steelant. Experimental investigation of the effect of steps and gaps on hypersonic vehicles. 2nd International Conference on High-Speed Vehicle Science and Technology (HiSST), 2022.
- [2] K. D. Fong, X. Wang, and X. Zhong. Numerical simulation of roughness effect on the stability of a hypersonic boundary layer. *Computers & Fluids*, 96:350–367, 2014.

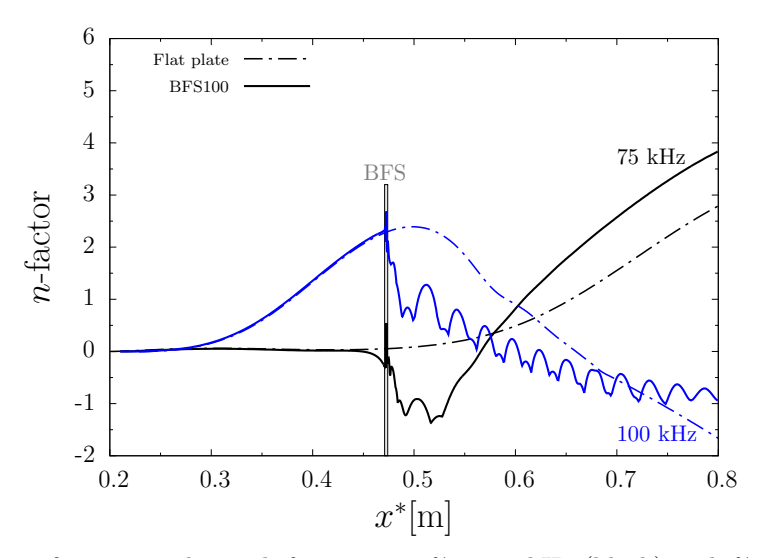


**Fig 5.** *n*-factor curves for two modes with frequencies  $f^* = 75$  kHz (black) and  $f^* = 100$  kHz (blue). Solid and point-dashed lines stand for BFS100 and flat-plate cases, respectively. The vertical grey line indicates the location of the BFS.

- [3] K. D. Fong, X. Wang, and X. Zhong. Parametric study on stabilization of hypersonic boundary-layer waves using 2-D surface roughness. *AIAA Paper 2015-0837*, 2015.
- [4] A. Fedorov. Transition and stability of high-speed boundary layers. *Annual Reviews Fluid Mechanics*, 43:79–95, 2011.
- [5] G. Gong, G. Tu, B. Wan, C. Li, J. Chen, and W. Hu. Response of second-mode instability to backward-facing steps in a high-speed flow. *Physics of Fluids*, 36(014122), 2024.
- [6] Q. Mi, S. Yi, X. Zhao, D. Gang, and X. Xu. Effects of backward-facing step shape on hypersonic flow characteristics. *Journal of Thermophysics and Heat Transfer*, 36(2), 2022.
- [7] K. Yu, J. Hao, C.-Y. Wen, and J. Xu. Bi-global stability of supersonic backward-facing step flow. Journal of Fluid Mechanics, 981(A29), 2024.
- [8] R. Zhao, C. Y. Wen, X. D. Tian, T. H. Long, and W. Yuan. Numerical simulation of local wall heating and cooling effect on the stability of a hypersonic boundary layer. *International Journal of Heat and Mass Transfer*, 121:986–998, 2018.
- [9] T. Zhou, Y. Lu, Z. Liu, and C. Yan. Direct numerical simulation of control of oblique breakdownn in a supersonic boundary layer using a local cooling strip. *Physics of Fluids*, 33(084101), 2021.
- [10] DLR. TAU-Code user guide, 2024. v.2024.1.0.
- [11] O. Brodersen, A. Ronzheimer, R. Ziegler, T. Kunert, J. Wild, and M. Hepperle. Aerodynamic applications using MegaCads. 6th International Conference on Numerical Grid Generation, 1998.
- [12] S. Hein, F. P. Bertolotti, M. Simen, A. Hanifi, and D. Henningson. Linear nonlocal instability analysis - the linear NOLOT code. Internal report IB 223-94 A56, DLR, 1995.
- [13] J. A. Franco and S. Hein. Adaptive harmonic linearized Navier-Stokes equations used for boundarylayer instability analysis in the presence of large streamwise gradients. AIAA Paper 2018-1548, 2018.
- [14] D. Arnal. Boundary layer transition: Predictions based on linear theory. Progress in transition modelling 793, AGARD, 1994.

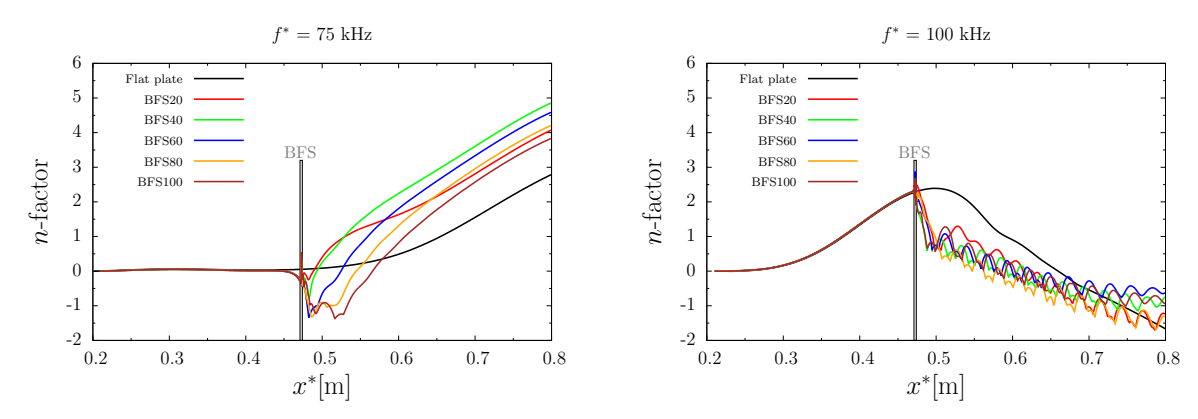
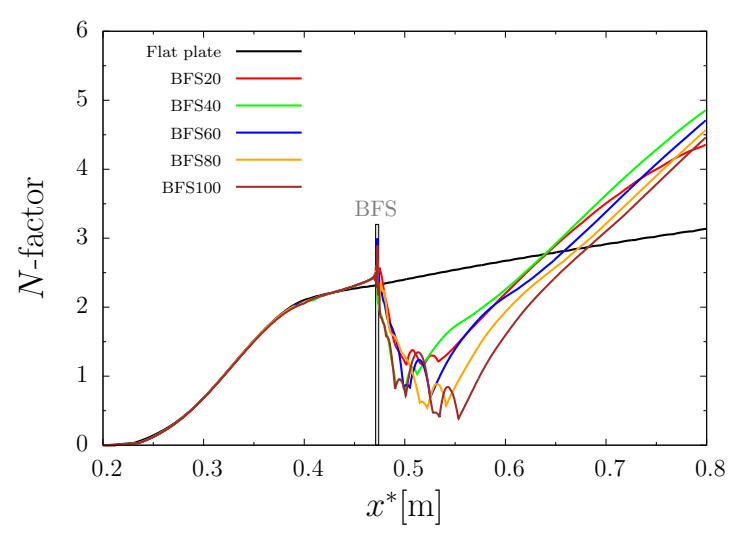


Fig 6. Influence of step height on the individual n-factor curve for modes with frequencies  $f^* = 75$  kHz (left) and  $f^* = 100$  kHz (right). The vertical grey line indicates the location of the BFS. The corresponding curve for the flat-plate case has been added for comparison.



**Fig 7.** N-factor envelope curves for the five steps of the study. The vertical grey line indicates the location of the BFS. The corresponding envelope for the flat-plate case has been added for comparison.

- [15] L. M. Mack. Boundary layer linear stability theory. Special course on stability and transition of laminar flow 709, AGARD, 1984.
- [16] J. A. Franco, A. Theiss, and S. Hein. Influence of surface irregularities on the expected boundary-layer transition location on hybrid laminar flow control wings. *New Results in Numerical and Experimental Fluid Mechanics*, XIII:174–184, 2021.